JOURNAL OF MATERIALS SCIENCE 35 (2000) 5899–5905

AC electrical conductivity of electron beam evaporated Cu-GeO_2 thin cermet films

M. H. RAHMAN
International Development Consultants. 25 Condie Street. Nepean, Ontario, Canada K2G 5M3
E-mail: rahman@kimep.kz

A. M. AI-SAIE
Department of Physics, University of Bahrain, P.O.Box 32038, Bahrain, Arabian Gulf

J. BEYNON
Department of Physics, Brunel University, Uxbridge, Middlesex, UB8 3PH UK

AC electrical properties of 410 nm thick 30 at.wt% Cu-70 at.wt% GeO_2 thin films are reported for the frequency range 10^4 to 10^6 Hz and temperature range 150 to 425 K. The loss tangent (tan δ) and the dielectric loss (ϵ''/ϵ_0) are found to show striking minima around a cut-off frequency $\sim 10^5$ Hz. In the lower frequency range ($\leq 10^5$ Hz), $\sigma_1(\omega) \propto \omega^s T^n$ is obeyed with s (0 to 0.51) increasing as a function of temperature and n (0.10 to 0.14) showing a very weak temperature dependence. In the higher frequency region ($\geq 10^5$ Hz), $\sigma_1(\omega)$ and ϵ''/ϵ_0 increase sharply leading to the quadratic behavior of $\sigma_1(\omega)$ with s equal to 2. These processes are discussed by analyzing an equivalent circuit which shows that at lower frequencies, the effects of series resistance in leads and contacts can be neglected, while at higher frequencies such effect give rise to spurious ω^2 dependance for the conductance. A weakly activated AC conductivity and a frequency exponent s that increases with increasing temperature suggest that the low frequency behavior originates from carrier migration by tunneling process.

1. Introduction

Cermet films are primarily insulators with metal incorporated. It is widely believed that a multicomponent system like the cermet film consists of discrete metal islands dispersed in a continuous insulating matrix [1–5]. Depending on the metal content, this material can have widely varying dielectric properties. Consequently it has found numerous and varied applications in electronics and optoelectronics devices [6, 7].

Most of the AC loss measurements reported for amorphous semiconductors showed pronounced loss peaks or loss minima in the frequency dependent loss tangent curves [8–13]. The origin of such behavior is generally ascribed to Debye-like dielectric polarization but there are good experimental and theoretical evidence that such behavior may also arise due to carrier hopping or tunneling between localized defect states within the energy gap [9, 14–24]. However, such interpretations are often complicated by the onset of direct current conduction at lower frequencies and by the presence of series resistance affects at higher frequencies [9, 19, 21]. Frequently these two affects lead to erroneous interpretations of the experimental data. Therefore, in any meaningful interpretation of the AC loss data, these must be carefully considered.

Our previous works on DC conductivity, Hall effects and optical absorption [25–27] reveal the existence of a large number of localized states and an impurity band in the mobility gap formed by the structural defects and impurities. Polaronic hopping was predicted to be the dominant conduction mechanism. Such inhomogeneties may act as prime sources of dielectric loss mechanism which could give rise to the low-frequency ($\leq 10^6$ Hz) universal behavior for the real part of the AC conductivity [14, 18, 19], viz.

$$\sigma_1(\omega) \propto \omega^s T^n \tag{1}$$

where ω is the angular frequency of the applied field, T is the absolute temperature, s is a temperature dependent quantity whose values lies within $0 < s \leq 1$, and n is the temperature exponent lying in the range 0.1 to 0.4. A careful temperature dependent study of the frequency exponent s is expected to be helpful in elucidating the microscopic dielectric relaxation mechanism responsible for the AC loss. In the present studies, the AC loss behavior was analyzed in terms of an equivalent-circuit, and the physical implications of such behavior were investigated from the temperature dependent studies of s.

2. Experimental techniques

2.1. Film preparation

410 nm thick 30 at.wt.% Cu-70 at.wt% GeO_2 films were deposited on ultrasonically cleaned Corning 7059 glass substrates by electron-beam evaporation from a single

graphite boat at a pressure $\approx 10^{-3}$ to 10^{-4} Pa. Prior to the deposition, Cu and GeO_2 powders were all mixed in a porcelain crucible and pressed in the shape of discs in vacuum under a pressure of 8 tons weight. The disc was then transferred to the evaporation chamber where it was melted in the graphite boat using electron beam with the mechanical shutter covering the source. This was done to ensure homogeneity of the mixture. The glass substrates were positioned centrally and the films were deposited onto them at a temperature of 303 K and a beam voltage of 4 KV corresponding to a beam current of 15 mA. The mean deposition rate (3 nm/s) and the thickness (t) were monitored insitu with the help of an Edwards FTM5 quartz crystal thickness monitor.

2.2. X-ray and IR measurements

The amorphous nature of the Cu-GeO_2 films and 100% GeO_2 sample was checked by X-ray diffraction measurements using a Phillips (model PW 1729) X-ray generator and by infrared absorption studies. Specimen for IR studies were evaporated on freshly cleaned and dried mono-crystalline silicon wafers doped with boron. Measurements were carried out at room temperature in the range 400 to 4600 cm^{-1} using a Nicolet (model 5 DX) infrared spectrometer. An uncoated silicon wafer substrate was used as a reference to eliminate any possible influence of the substrate.

2.3. Conductance and capacitance measurements

Aluminum electrodes of dimensions 4.5 mm × 2 mm with a gap of 1.5 mm between them were thermally evaporated onto the films to produce a coplanar geometry. The main advantage of using a coplanar geometry is that the large sheet resistance (about 10^{10} Ohms at room temperature) generally masks any contact effect and the substrate contribution to the AC loss becomes very small [19, 24]. Since the film thickness t (410 nm) is much less than the electrode separation d (1.5 mm), the field distribution in the gap may be assumed uniform. Ohmic contacts were checked using a Keithley 220 constant current source and a high impedance Keithley 617 electrometer.

All electrical measurements were taken inside DN 1714 (Oxford Instrument) variable temperature liquid nitrogen cryostat at a pressure $\approx 10^{-2}$ Pa. The temperature of the samples was varied in the range 150 to 425 K (within an uncertainty of about 5%) using a ITC4 temperature controller. A 0.8 $V_{r.m.s.}$ was applied to the sample. The conductance (G), capacitance (C), loss tangent (D) and the quality factor (Q) were all measured in the frequency range 10^4 to 10^6 Hz using an HP 4275A LCZ meter in the two-terminal configuration. The HP LCZ meter measures these parameters with a basic accuracy of ±0.1 to 5%. In the lower frequency range (10^4 to 10^5 Hz) there was a 10 to 20% uncertainty in the values of C, G and D whereas in the higher frequency range all readings were stable. Thus, readings were first taken in ascending order of frequency and later the steps were repeated in descending order. No significant differences were observed in the two sets of readings. Furthermore, the samples were left overnight and the reproducibility of the measurements were checked the following morning. Again no significant dispersion of the measurements were observed.

Measurements were made in the parallel-mode as shown in Fig. 1a. A digital offset adjustment function measured the stray capacitance (0.0002 pF) and the residual resistance r (∼5 Ω) inherent to the leads and the test fixtures, and automatically eliminated these parasitic effects with respect to the measured values.

3. Results

3.1. X-ray and IR studies

Fig. 2 shows the scans from 10° to 65° (2Θ) for the sample and the glass substrate. The scans clearly indicate the amorphous nature of the sample. A broad hump was noticed at $2\Theta = 23^\circ$ for the glass substrate. For the Cu-GeO_2 sample, the hump became diminished signifying that the observed spectrum is mainly due to the film.

Fig. 3 shows the infrared absorption spectra for Cu-GeO_2 and 100% GeO_2 films. No vibrational modes were observed in this range. Furthermore, spectra for Cu-GeO_2 film is practically identical to that of the GeO_2 film. Because GeO_2 is known to be an amorphous

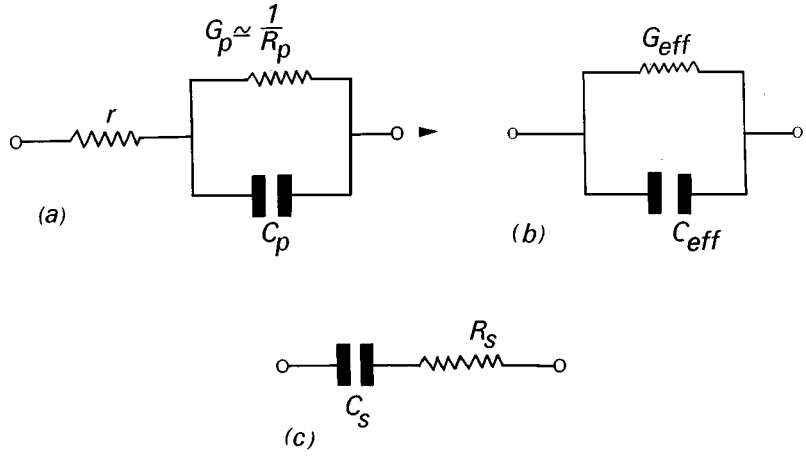

Figure 1 (a) Three element parallel mode; (b) Two element effective parallel mode; (c) Two element equivalent series mode.

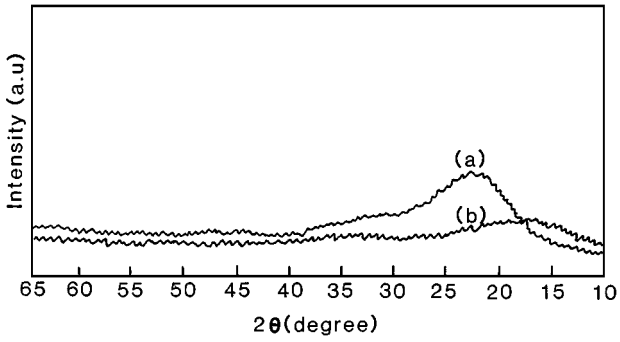

Figure 2 X-ray diffraction spectra of (a) Corning 7059 glass substrate; (b) Cu-GeO_2 film.

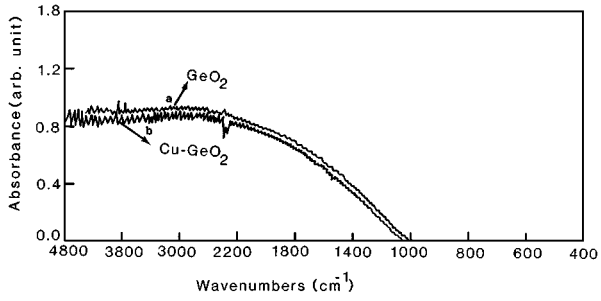

Figure 3 Infrared absorption spectra of (a) 100% GeO_2 film; (b) Cu-GeO_2 film.

material, the identical spectra suggest that film is also amorphous in nature and the cermet matrix is dominated by GeO_2 component. Interestingly, this conclusion, and that this composition is well below the percolation threshold were reached from our previous works on DC conductivity and Hall effects [25, 26].

3.2. Variation of capacitance, loss tangent and dielectric loss with frequency and temperature

Figs 4 and 5 show the variation of capacitance with frequency at different temperatures and the variation with temperature at different frequencies, respectively. The magnitude of the capacitance at a given temperature and frequency lies within the range 1.13×10^{-13} to 1.25×10^{-13} F. It decreases slightly as frequency

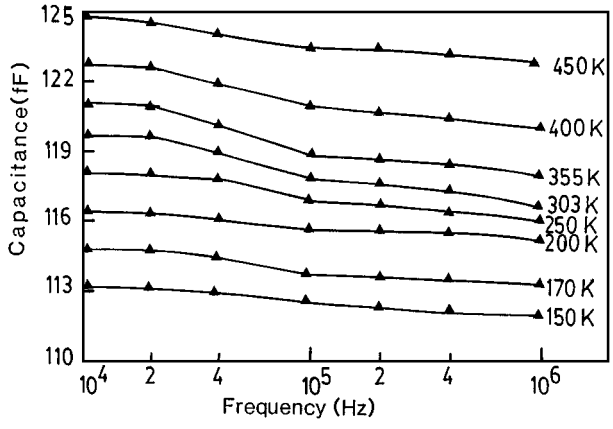

Figure 4 Variation of capacitance with frequency at different temperatures.

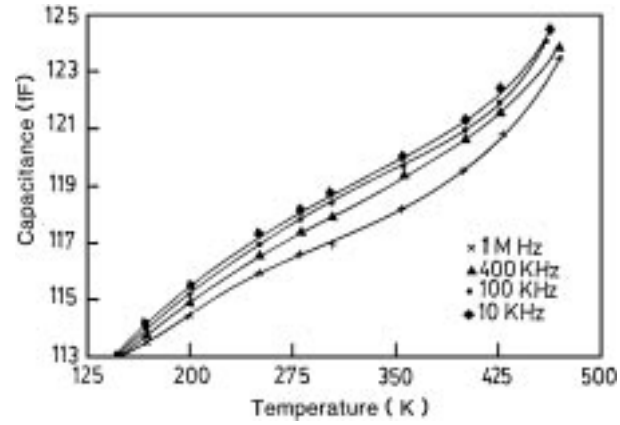

Figure 5 Variation of capacitance with temperature at different frequencies.

is increased to 10^5 Hz. The decrease is more prominent at lower frequencies and higher temperatures. At higher frequencies ($\geq 10^5$ Hz) and lower temperatures ($\leq$250 K), capacitance shows very little dependance on frequency. Fig. 5 shows that capacitance increases as temperature is increased at all frequencies. Throughout the entire temperature range (150 to 425 K), capacitance shows a weak frequency-dependance.

The variation of loss tangent (tan δ) with frequency is shown in Fig. 6: it consists of two frequency regions. In the lower frequency region (10^4 to 10^5 Hz), the loss factor decreases sharply, showing two loss minima over a relatively narrow range, $\omega_m = 10^4$ to 2×10^5 Hz. Beyond these, tan δ increases rapidly with frequency. Values of ω_m and tan δ shift towards slightly higher values with increase in temperature. It will be shown in section (4.1) that a minimum in tan δ vs frequency data has no particular physical significance but which can be related to a straight forward equivalent circuit analysis.

The real part of the dielectric constant (ϵ'/ϵ_0) was calculated from the geometry of the sample. The dielectric constant (ϵ''/ϵ_0) also known as dielectric loss, was calculated from the values of (ϵ'/ϵ_0) and tan δ using the relation,

$$\tan \delta = \frac{\epsilon''}{\epsilon'} \qquad (2)$$

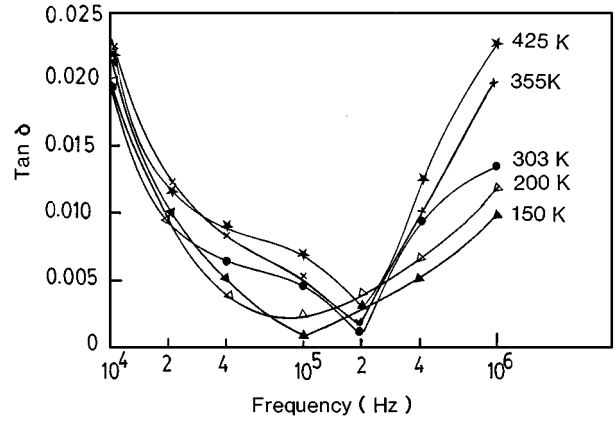

Figure 6 Variation of loss tangent with frequency at different temperatures.

TABLE I Values of the AC loss parameters at 150 K

f(kHz)	n at 150–425 K	W(eV) at 150–425 K	σ_1(S m^{-1}) at 150 K	ϵ''/ϵ_0
10	0.10	1.1×10^{-3}	1.7×10^{-4}	294.9
20	0.10	2.7×10^{-3}	1.6×10^{-4}	136.7
40	0.14	3.0×10^{-3}	1.5×10^{-4}	70.3
100	1.40	30×10^{-3}	1.1×10^{-4}	9.8
200	0.57	11×10^{-3}	6.5×10^{-4}	56.2
400	0.70	18×10^{-3}	15×10^{-4}	70.4
1000	0.78	20×10^{-3}	79×10^{-4}	140.0

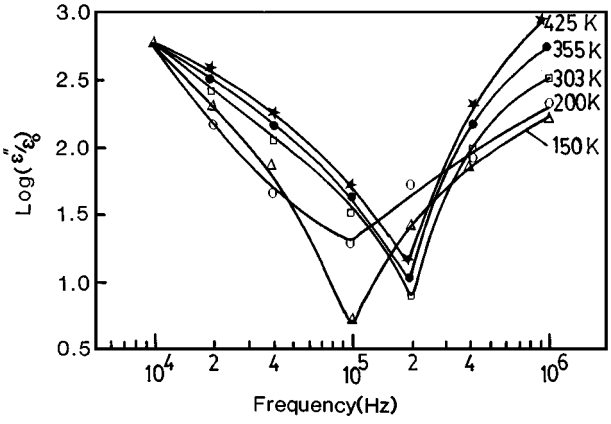

Figure 7 Frequency dependence of dielectric loss (ϵ''/ϵ_0) at different temperatures.

where ϵ' and ϵ'' are the real and imaginary components of the effective permittivity $\epsilon(\omega)$ respectively. Some typical values (at 150 K) are listed in Table I. The real part of the conductivity $\sigma_1(\omega)$ can be expressed in terms of the dielectric loss by,

$$\epsilon'' = \frac{\sigma_1(\omega)}{\omega} \tag{3}$$

Using Equation 1, Equation 3 can be re-written as,

$$\epsilon''(\omega) = \omega^{s-1} T^n \tag{4}$$

Fig. 7 shows the variation of log (ϵ''/ϵ_0) with frequency at a given temperature. It shows a similar frequency-dependence as that of tan δ (Fig. 6). Table II shows the values of s estimated from the slope $(s-1)$ of Fig. 7 as a function of temperature for the two frequency regions.

TABLE II The frequency exponent S calculated from Figs 7 and 8 at different frequency regions. $\bar{S}$ represents the average value used in Fig. 10

	10^4 to 10^5 Hz			10^5 to 10^6 Hz		
Temp (K)	S Fig. 8	$(S-1)$ Fig. 7	$\bar{S}$	S Fig. 8	$(S-1)$ Fig. 7	$\bar{S}$
150	0	−1.0	0	1.82	1	1.91
170	0	—	0	1.74	—	1.74
200	0.1	−0.9	0.1	1.61	0.77	1.69
250	0.35	−0.75	0.30	1.50	0.65	1.58
303	0.42	−0.59	0.41	1.39	0.70	1.54
355	0.45	−0.56	0.44	1.45	—	1.45
400	0.62	−0.61	0.50	1.69	0.82	1.75
425	0.63	−0.61	0.51	1.81	0.70	1.76

3.3. Variation of the AC conductivity with frequency and temperature

The magnitude of the conductance G_p at a given temperature and frequency was found to lie in the range 0.16 to 15 nS. Since the sheet resistance of the material is very high and the lead resistance r very low, a simple impedance calculation shows that G_p is effectively equal to 1/Rp. Taking the given geometry of the samples, the measured conductivity $\sigma_p(\omega)$ was calculated in the range 10^{-5} to 10^{-2} S m^{-1}. However, it is known that AC loss is always accompanied by a DC component at $T > 0$ K [9, 18, 19]. Consequently the DC component must be carefully subtracted from $\sigma_p(\omega)$ to obtain $\sigma_1(\omega)$. For this reason, the zero-frequency DC conductivity was measured in the same temperature range i.e. 150 to 425 K.

At high temperatures and low frequencies the DC conductivity becomes comparable with $\sigma_p(\omega)$ and therefore, $\sigma_1(\omega)$ can be extracted from $\sigma_p(\omega)$ using

$$\sigma_1(\omega) = \sigma_p(\omega) - \sigma_{d.c.} \tag{5}$$

However, at lower temperatures, ($T < 303$ K), the AC conductivity completely dominates the DC conductivity at all frequencies and, as such, no subtraction was necessary. Fig. 8 shows the frequency dependence of $\sigma_1(\omega)$ at different temperatures. Two distinct frequency regions similar to those of Figs 6 and 7 are visible. This behavior suggests that the AC loss in these films may arise from different physical processes, and that a single universal power law behavior may not be appropriate for the entire frequency range.

The frequency exponent s was determined from the slopes of Fig. 8 and, with values determined earlier from the slopes of Fig. 7, an average value was calculated. Table II shows the average values of s as a function of frequency in the two frequency regions. At low temperatures (150 to 200 K) and frequencies (10^4 to 10^5 Hz), conductivity shows an almost frequency independent behavior with $s \sim 0$. At $T > 200$ K, $\sigma_1(\omega)$ shows a slight increase as frequency is increased towards the cut-off value; s increasing in the range 0.30 to 0.51. At higher frequencies ($\geq 10^5$ Hz) Fig. 8 shows that $\sigma_1(\omega)$ increases rapidly with frequency at all temperatures. Over this range, AC conductivity seems to follow a square law behavior (i.e. $\sigma_1(\omega) \propto \omega^2$ with s lying in the range 1.45 to 1.91.

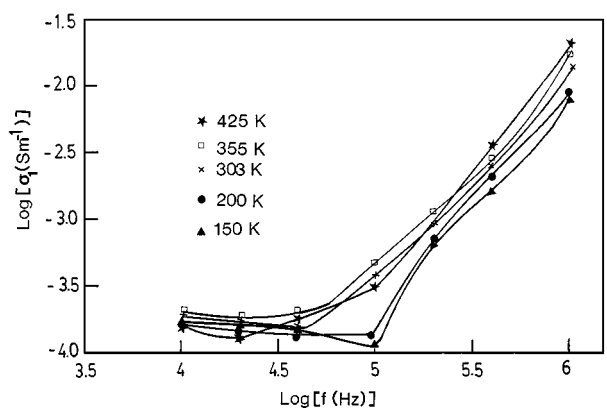

Figure 8 Frequency dependence of $\sigma_1(\omega)$ at different temperatures.

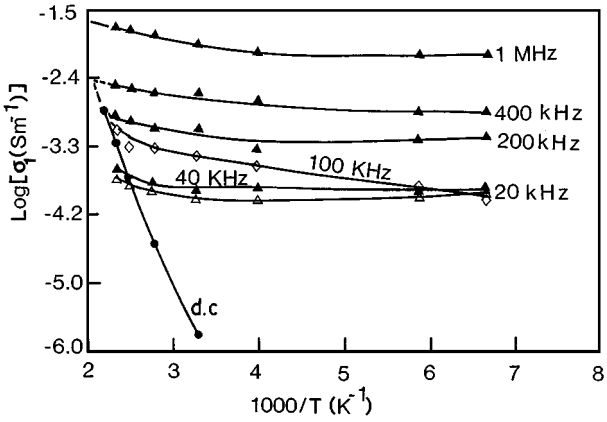

Figure 9 $\sigma_1(\omega)$ Plotted as a function of $1000/T$ at different frequencies.

Fig. 9 shows the temperature-dependence of $\sigma_1(\omega)$ at different frequencies. At low temperatures and at frequencies below ω_m, the AC conductivity shows a very weak temperature-dependence; the temperature exponent n lying in the range 0.10 to 0.14. The resulting curves indicate that the real part of the AC can be written as

$$\sigma_1(\omega) \approx \sigma_0 \, e^{-W/kT} \tag{6}$$

where W is the thermal activation energy. Fig. 9 yields the values of W in the range 1.1×10^{-3} to 30×10^{-3} eV. It is found to vary considerably with frequency but negligibly with temperature. At 10^5 Hz, $\sigma_1(\omega)$ shows a stronger temperature-dependence, with $n = 1.40$ corresponding to increased activation energy of 0.03 eV. Above the cut-off frequency, the temperature-dependence is seen to decrease, with a consequent decrease in activation energies. The values of n and W at different frequencies and temperatures, and some typical values of $\sigma_1(\omega)$ at 150 K are listed in Table I.

4. Discussion

4.1. Frequency and temperature dependence behavior of Loss tangent and dielectric loss

In planar geometry, the dielectric loss is though to be partially governed by the substrate contribution. This was tested by measuring the response of a bare substrate with electrodes where it was found that the substrate contributions to C, G, and tan δ were about 30%. It is uncertain, however, to what extent this affects the actual measurements on a cermet-glass substrate composite system. Furthermore, no minimum was observed in the spectral behavior of G and tan δ. It has been argued [19, 24,] that if the film thickness (t) is much less than the thickness of the glass substrate, then the electric field-penetration into the substrate may be negligible. Since in the present work the film thickness t (410 nm) is much less than the substrate-thickness (2 mm), it is assumed that the observed temperature or frequency dependence of the dielectric response is largely due to the film.

Some of the AC loss features observed in Figs 4–7 are in conformity with those observed in thin films of ZnS [8], SiO/SnO_2 [10] and Copper phthalocyanine [12]. A qualitative analysis of the situation may be presented interms of Goswami-Goswami model [8] in which Fig. 1a is first converted to an effective parallel mode (Fig. 1b) and then to a two element series circuit mode (Fig. 1c). At a given frequency the circuits in Fig. 1b and c have equal impedance i.e. $Z_{eff} = Z_s$. Equating the real and imaginary parts of series impedance ($Z_s = R_s + 1/j\omega C_S$) and effective parallel-mode impedance ($Z_{eff} = r + R_p/(1 + j\omega C_p R_p)$), Goswami and Goswami [8] obtained the following relationship between series and parallel mode parameters, viz.

$$C_S = \frac{1 + \omega^2 R_P^2 C_P^2}{\omega^2 R_P^2 C_P^2} = (1 + D^2) C_P \tag{7}$$

and

$$R_S = r + \left(\frac{D^2}{1 + D^2}\right) R_P \tag{8}$$

Here, C_S and R_S are the equivalent series capacitance and resistance, respectively, of the circuit mode in Fig. 1c. C_P is the inherent capacity element of the circuit in Fig. 1a unaffected by frequency and temperature. R_P is the discrete resistance element due to the dielectric film and is unaffected by temperature. D is the diffusion factor of the parallel circuit mode in (Fig. 1a) and is equal to

$$\frac{1}{\omega R_P C_P}.$$

Taking $\tan \delta = \omega \, R_S \, C_S$, for the equivalent circuit of Fig. 1c, and using Equations 7 and 8, Goswami and Goswami [8] and Tareev [13] derived, in the limit $r/R_p \ll 1$,

$$\tan \delta = \frac{1}{\omega R_P C_P} + \omega r C_P \tag{9}$$

Equation 9 suggests that tan δ has a minimum at a frequency given by,

$$\omega_m = \left(\frac{1}{r R_P C_P^2}\right)^{1/2} \tag{10}$$

Equation 7 predicts the behavior of C_S as observed in Figs 4 and 5. At a given temperature, $D(=1/\omega C_P R_P)$ decreases with increasing frequency leading to a decrease in C_S whereas at given frequency, D increases with rising temperature leading to an increase in C_S.

The frequency dependence of tan δ (Fig. 6) and dielectric loss ϵ''/ϵ_0 (Fig. 7) is in conformity with the predictions of Equation 9. In each case, there is an identical transition frequency. Below ω_m, these parameters show a monotonic decrease with increasing frequency while above ω_m they increase rapidly. Such two power-law

behavior has frequently been observed in many amorphous materials [8–10, 13, 14]. Equation 10 indicates that with increasing temperature (as R_P decreases), ω_m should shift towards higher values; a feature partially observed in Cu-GeO_2 thin films (see Figs 6 and 7). Although no maxima has been observed in this frequency range, there is a strong possibility that the spectral behavior in Figs 6 and 7 result from the overlap of two maxima; one off-scale at a lower ($<10^4$ Hz) and the other off-scale at a higher frequency ($>10^6$ Hz) range. Therefore, the temperature dependence of ω_m reflects the different temperature dependence of the low and high frequency maxima plus any temperature variation in the spread of the two loss peaks and minima.

4.2. Frequency and temperature dependence behavior of AC conductivity

The behavior of the AC conductivity data (Fig. 8) may be analyzed in a similar fashion to that of tan δ. Fig. 1a represents a physical situation whereby the AC conductivity is affected by a finite contribution from DC conductivity. The parallel mode admittance $Y_P(\omega)$ is given by,

$$Y_P(\omega) = G_P(\omega) + j\omega C_P \tag{11}$$

The conductance $G_P(\omega) \sim 1/R_P$ does not include any contribution from lead and contact resistance r. It is widely believed, however, that the effective conductance $G_{eff}(\omega)$ should have a contribution from r and that it is this effect which leads to the $s > 1$ behavior [19, 21]. In order to investigate this behavior, we begin by defining an effective admittance for the circuit in Fig. 1b,

$$Y_{eff}(\omega) = G_{eff}(\omega) + j\omega C_{eff}(\omega) = \frac{1}{Z_{eff}} \tag{12}$$

Substituting the expressions for Z_{eff} into Equation 12, one obtains,

$$Y_{eff}(\omega) = \frac{(r + R_P) + \omega^2 C_P^2 R_P^2 r + j\omega C_P R_P (r + R_P)}{(r + R_P)^2 + \omega^2 C_P^2 R_P^2 r^2} \tag{13}$$

Equating the real parts of Equations 12 and 13, one obtains,

$$G_{eff}(\omega) = \frac{(r + R_P) + \omega^2 C_P^2 R_P^2 r}{(r + R_P)^2 + \omega^2 C_P^2 R_P^2 r^2} \tag{14}$$

Equation 14 has two important consequences. In the lower frequency region ($\leq \omega_m$) and, assuming that $r/R_P \ll 1$ in all cases, this equation becomes,

$$G_{eff}(\omega) = \frac{\left(\frac{1}{R_P^2}\right)}{\left(\frac{1}{R_P}\right)} = \left(\frac{1}{R_P}\right) = G_P(\omega) \tag{15}$$

Equation 15 suggests that at lower frequencies effective conductance is not affected by the series lead and contact resistance. However, when the frequency is increased towards ω_m, so that $\omega_m^2 C_P^2 R_P r = 1$ (Equation 10) condition is satisfied, then $G_{eff}(\omega)$ begins to rise above G_P. This can be seen by dividing the numerator and denominator of the Equation 14 by R_P^2. In the limit $r/R_p \ll 1$, Equation 14 can rewritten as

$$G_{eff}(\omega) = \frac{\left(\frac{1}{R_P}\right) + \omega^2 C_P^2 r}{1 + \omega^2 C_P^2 r^2} \tag{16}$$

Using $\omega_m^2 C_P^2 r R_P = 1$, the above expression becomes, in the limit $r/R_p \ll 1$

$$G_{eff}(\omega) = G_P(\omega) + \omega^2 C_P^2 r \tag{17}$$

Separating AC and DC contributions in $G_P(\omega)$ according to Equation 5, and using Equation 1 for $\sigma_1(\omega)$, Equation 17 can be written as

$$G_{eff}(\omega) = G_{d.c.}(T) + \omega^S T^n + \omega^2 C_P^2 r \tag{18}$$

Equation 18 clearly shows that different physical processes are responsible for the origin of conductivity. At lower frequencies, the contribution from r can be neglected for very low capacitive materials. In this case, the first two terms are expected to dominate the conductance, with s taking values in the range $0 < s \leq 1$. The temperature of observation at a given frequency determines which of these two terms are dominant. At higher frequencies (e.g. $\omega \geq \omega_m$), the effect of r becomes significant and hence, the third term may dominate the overall conductivity.

In the present investigation, the high frequency AC conductivity shows a quadratic behavior with s ($\sim$1.45 to 1.91) slightly deviating from the predicted value of 2. It is therefore believed, in view of Equation 18, that high frequency square law behavior originates from spurious series and contact resistance effects. We now look at the physical origin of the low frequency behavior i.e. the middle term in Equation 18. As mentioned in section 1, this term may be associated with microscopic relaxation process associated with carrier tunneling between localized states. Fig. 7 shows that the dielectric loss factor reaches a minimum at a frequency given by Equation 10. This feature seems to be in conformity with small polaron tunneling process which predicts a sharp peak or minimum in the loss curves if the dielectric polarization is due to carrier migration through localized states formed by structural defects and impurities [9, 18, 19]. Other important signatures of the tunneling process can be found in the temperature dependence of the frequency exponent s [16, 19, 28], and in the magnitude of the thermal activation energy [19]. In the tunneling model, assuming the universal behavior in Equation 1, the frequency exponent s is given by [19],

$$S = 1 + \frac{4}{[\ln(\omega\tau_{ot}) + W/kT]} \tag{19}$$

where τ_{ot} is the constant characteristic relaxation time for small polaron tunneling. Equation 19 predicts an

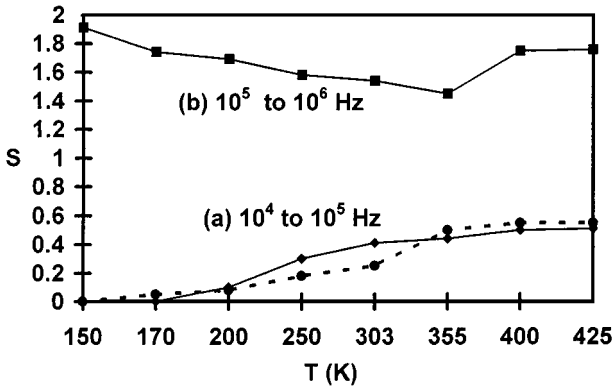

Figure 10 Temperature dependence of the exponent S at different frequency regions; (a) 10^4 to 10^5 Hz. The dotted curve is calculated using Equation 19; (b) 10^5 to 10^6 Hz.

exponent s which increases with temperature in the range $0 < s \leq 1$. The temperature dependence of s is shown in Fig. 10 (curve a); s is an increasing function of temperature in agreement with Equation 19. Furthermore, the characteristic constant relaxation time (τ_{ot}) predicted by this model $\sim 10^{-8}$ to 10^{-7} s. Taking the values of W from Table I, the frequency exponent s was calculated using Equation 19. The dotted line in Fig. 10 represents these calculated values, which is in excellent agreement with experimental solid-line. Fig. 9 shows that the AC conductivity $\sigma_1(\omega)$ is weakly activated with $W \sim 10^{-3}$ eV and $n \sim 0.10$ to 0.14. Such relatively low activation energies are also the characteristics of the electrical conductivity occurring via small polaron tunneling within a dominant constituent [18, 19, 29, 30].

Fig. 10 (curve b) shows the super linear behavior of s (>1) in the higher frequency region. The almost flat nature of the curve suggests a weakly varying s with temperature and frequency. Such behavior has been reported many times in the literature [9, 10, 12, 18–21]. There does not appear to be much clear and conclusive experimental evidence for the origin of this behavior. Equation 18 predicts that such behavior for the conductance arises from the spurious effects related to series lead and contact resistance. However, Mott and Davis [20] predicted that such behavior may also arise from the resonant absorption of a photon from the applied field. Analysis of the resonant process suggests that in the high frequency region where $h\upsilon \gg kT$, the loss will vary as ω^2 and that the frequency exponent s (~ 2) may itself be a function of temperature [18]. In this case $\sigma_1(\omega)$ is expected to show considerable variation with temperature. In the present work the photon energy is found to be significantly lower than the thermal energy at all temperatures, and the AC conductivity shows negligible variation with temperature at all frequencies (Fig. 8). These observations lead us to believe that the resonant process is unlikely to be important in the frequency range used in this work.

5. Conclusion

The equivalent circuits in Fig. 1b and c seem to describe the behavior of the observed capacitance, tan δ, dielectric loss and $\sigma_1(\omega)$ accurately. The frequency and temperature dependence of the capacitance and tan δ is in conformity with the predictions of Equations 7 and 9, respectively. The frequency dependence of the AC conductivity appears to agree well with the two power-law behavior predicted by Equation 18; at lower frequencies Equation 1 is obeyed with $s < 1$, while at higher frequencies the conductivity shows a square law behavior. The existence of sharp loss minima, a low activation energy at all temperatures and a frequency exponent s which increases with temperatures, are all features which suggest that the low frequency conduction mechanism occurs via small polaron tunneling. At higher frequencies, the square law behavior of the conductivity arises mainly due to spurious effects related to series lead and contact resistance.

References

1. C. A. NEUGEBAUER and M. B. WEBB, *J. Appl. Phys.* **33**(1) (1962) 74.
2. T. J. COUTTS, *Thin Solid Films* **4** (1969) 429.
3. J. E. MORRIS, *ibid.* **11** (1972) 199.
4. R. M. HILL and T. J. COUTTS, *ibid.* **42** (1977) 201.
5. P. SHENG, *Phil. Mag.* **B65** (1992) 357.
6. K. L. CHOPRA, S. MAJOR and D. K. PANDYA, *Thin Solid Films* **102** (1983) 1.
7. M. OHRING, "The Materials Science of Thin Films" (Academic Press Inc, New York, 1992) p. 508 and p. 629.
8. A. GOSWAMI and A. P. GOSWAMI, *Thin Solid Films* **16** (1973) 175.
9. A. K. JONSCHER, in "Dielectric relaxation in solids" (Chelsea Dielectric Press, London, 1983) p. 192 and p. 225.
10. A. S. M. RAHMAN, M. H. ISLAM and C. A. HOGARTH, *Int. J. Electronics* **62**(2) (1987) 167.
11. M. H. ISLAM and C. A. HOGARTH, *J. Mat. Sc.* **24** (1989) 4392.
12. R. D. GOULD and A. K. HASSAN, *Thin Solid Films* **223** (1993) 334.
13. B. TAREEV, in "Physics of Dielectric Materials" (Mir Publishers, Moscow, 1975) p. 78.
14. A. K. JONSCHER, *Thin Solid Films* **36** (1976) 1.
15. G. E. PIKE, *Phys. Rev.* **B6** (1972) 1572.
16. S. MANDAL and A. GHOSH, *J. Phys: Condens. Matter* **7** (1995) 9543.
17. S. R. ELLIOTT, *Phil. Mag.* **36** (1977) 1291.
18. *Idem., Adv. Phys.* **36**(2) (1987) 135.
19. A. R. LONG, *ibid.* **31**(5) (1982) 553.
20. N. F. MOTT and E. A. DAVIS, in "Electronic Processes in Non-Crystalline Materials," 2nd ed. (Clarendon Press, Oxford, 1979).
21. A. I. LAKATOS and M. ABKOWITZ, *Phys. Rev.* **B3** (1971) 1791.
22. J. HAUSER, *ibid.* **B27** (1983) 2543.
23. *Idem., ibid.* **B31** (1985) 2133.
24. K. L. NARASIMHAN, S. GUHA and S. C. AGARWAL, *Sol. St. Comm.* **20** (1976) 573.
25. A. M. AL-SAIE, M. H. RAHMAN and J. BEYNON, *J. Mater. Sci.* **28** (1993) 3675.
26. M. H. RAHMAN, A. M. AL-SAIE and J. BEYNON, *Int. J. Electronics* **76**(5) (1994) 929.
27. *Idem., Phys. Status. Solidi. (a)* **156** (1996) 397.
28. A. GOSH, *Phys. Rev.* **B42** (1990) 5665.
29. D. EMIN, in "Electronic and Structural Properties of Amorphous Semiconductors," edited by P. G. Le Comber and J. Mort (Academic Press, London and New York, 1973) p. 261.
30. I. G. AUSTIN and N. F. MOTT, *Adv. Phys.* **18** (1969) 41.

Received 20 October 1999
and accepted 8 May 2000